Water Practice & Technology

IWA PUBLISHING

Water Practice & Technology Vol 16 No 4, 1128 doi: 10.2166/wpt.2021.058

Efficient trapping of cesium ions in water by titanate nanosheets: experimental and theoretical studies

Luyao Lin, Ye Li*, Jie Wan, Cong Liu, Xiaoli Wang and Yixin Yin

School of Resources and Environmental Engineering, Wuhan University of Technology, Wuhan, Hubei 430070, China
*Corresponding author. E-mail: whly1218@126.com

ABSTRACT

In recent years, TNS has attracted wide attention because of its simplicity in synthesis and high efficiency in ion exchange. The adsorption of cesium ions in aqueous solution by TNS was investigated in this study. Results show that the removal rate of Cs (I) is about 88% when pH = 5.00 ± 0.05, C_0 = 10 ppm and C_{TNS} = 0.1 g/L. The adsorption equilibrium is reached in about 20 minutes and best fits the pseudo-second order model, R^2 = 0.9998; compared with the Freundlich isotherm adsorption model and Temkin model, the Langmuir model has the best fitting effect, R^2 = 0.9903. The fitting results show the maximum adsorption capacity of TNS for Cs (I) is 200.00 mg/g. The main adsorption mechanism of TNS to cesium ion is ion exchange. Therefore, TNS can be used as a potential adsorbent for effectively adsorbing Cs-containing wastewater.

Key words: adsorption, cesium, mechanism of action, titanate nanosheet

HIGHLIGHTS

- The removal of Cs (I) from aqueous solutions by TNS was firstly studied.
- TNS showed a high adsorption capacity for Cs (I).
- The solution pH played a significant role in the adsorption process of Cs (I).
- TNS exhibited an excellent selectivity for Cs (I) in the interference of common cations.
- The adsorption mechanism was the ion exchange between the interlayer Na (I) of TNS and Cs (I).

1. INTRODUCTION

In the environment, radioactive materials inevitably produce harmful radiation to organisms, and the permanent damage caused by radioactive cesium at the cellular level may cause cancer, genetic mutations, genetic diseases and other diseases (Sangvanich *et al.* 2010b; Thammawong *et al.* 2013; Kadam *et al.* 2016; Debnath *et al.* 2017). Persistent cesium also accumulates through the food chain and eventually poses a threat to humans. In the radioactive wastewater, 137Cs is a toxic nuclide with a half-life of 30.17 years, so the treatment of Cs pollution is urgent. The chemical properties of 137Cs are similar to potassium and sodium, so the radionuclide 137Cs in the water body mainly exists in the form of Cs (I) rather than elemental matter (Yi *et al.* 2014; Grandjean *et al.* 2016; Li *et al.* 2016).

At present, the methods for removing low-concentration cesium in wastewater mainly include chemical precipitation (Abusafa & Yücel 2002; Thammawong *et al.* 2013) ion exchange (Iwanade *et al.* 2012), solvent extraction method (Chen 2007), membrane separation (Zakrzewska-Trznadel *et al.* 2001), electrochemical method (Chen *et al.* 2013), adsorption, and so on. Among them, the inorganic ion exchange adsorbent has better mechanical properties, the ion exchange position is more uniform, and the adsorption selectivity for metal ions is high. Therefore, it has been often studied in the treatment of high level liquid waste. Commonly used inorganic adsorbents mainly include inorganic minerals (Chen & Li 2019), heteropoly acid salts (Zhang & Tan 2013), metal ferricyanide (Jiang *et al.* 1995), hydrous metal oxides (Thanabalasingam & Pickering 1990), iron-based composite materials (Pekárek & Veselý 1972) and so on. With the rapid development of nanotechnology, many researchers have begun to pay attention to the development of new nanomaterials, such as nanosheets, nanotubes, and several hybrid nanocomposites as adsorbents to remove heavy metals from wastewater (Deb *et al.* 2020). The abundance of active sites makes these nanoparticles potential adsorbents for the removal of radioactive contaminants from aqueous media (Bhowmik *et al.* 2019; Debnath *et al.* 2020). In

recent years, titanate nanomaterials have developed in the field of adsorption due to their wide range of raw materials and low prices, simple synthesis process, and unique physical and chemical properties such as large specific surface area. Various forms of titanate nanomaterials have been synthesized and applied to the field of heavy metal adsorption. After the first discovery that TiO_2 has a strong adsorption capacity for radioactive uranium (Amadelli *et al.* 1992), the scientific community discovered that titanate nanomaterials also have excellent adsorption effects on radionuclides in water. The adsorption effect of the synthesized anatase TiO_2 on more than ten kinds of metal cations proves that the TiO_2 series materials can quickly adsorb a large amount of cations (Vassileva *et al.* 1996). Through the study of titanate nanotubes and protonated titanate nanotubes, titanate nanomaterials were found to have a large number of exchangeable cations between the layers, and there are abundant adsorption sites on the surface, which can quickly adsorb and remove nuclide ions in water (Yang *et al.* 2003). However, the adsorption effect of TNS on Cs (I) has not been reported before. Therefore, in this study, a layered titanate material was prepared using titanium dioxide and sodium chloride as raw materials, and the adsorption capacity for Cs (I) was increased by increasing its specific surface area. For the adsorption capacity for cesium the layered titanate nanomaterials were used as adsorbents to study its adsorption characteristics for cesium, which provides a new idea for removing cesium from water in the future.

2. EXPERIMENTAL WORK

2.1. Materials used in the experiment

Nano titanium dioxide (TiO_2), sodium hydroxide (NaOH), ethanol (C_2H_6O), cesium chloride (CsCl), ammonia ($NH_3{\cdot}H_2O$), hydrochloric acid (HCl).

2.2. Preparation of TNS

0.8 g of nano titanium dioxide (TiO_2) and 25.6 g of sodium hydroxide (NaOH) were accurately weighed into a 250 mL beaker, and then 80 mL of ultrapure water was added into the beaker with a measuring cylinder and stirred for 12 h. The beaker was placed in an ultrasound machine for 12 hours, and then transferred to a 100 mL ptFE reactor and reacted in an oven at 130 °C for 3 hours. After the reaction, the products were centrifuged, cleaned with anhydrous ethanol and ultra-pure water 3 times respectively, and dried in a vacuum drying oven at 60 °C to obtain titanate nanometer tablets. The dried titanate nano-flakes were ground into fine powder, then sieved through 100 mesh, then put into a sample bag, and stored in the dryer for later use.

2.3. Batch adsorption experiments

In order to determine cesium ion adsorption, a cesium solution with a concentration of 5–40 mg/L was prepared from cesium chloride. In the intermittent adsorption experiment, a 250 mL glass conical flask was used, and 0.01 g TNS was added to 100 mL Cs(I) solution with an initial concentration (C_0) of 5–40 mg/L.The reaction temperature of 25 °C, stirring speed of 150 RPM and time of 2 h were selected. The suspension was then filtered by a 0.45 m filter, and the amount of cesium ions in the liquid phase before and after adsorption was determined by atomic absorption spectrometry. The adsorption capacity and removal rate of metal ions were obtained by the following method:

$$Q_e = (C_0 - C_e) \times V/m \tag{1}$$

$$R = (C_0 - C_e)/C_0 \times 100\% \tag{2}$$

where Q_e is the adsorption capacity (mg/g), V is the volume of the solution (mL), and m is the mass of TNS (mg); R is removal percentage of Cs (I) (%), C_0 is the initial Cs (I) concentration (mg/L), C_e is the equilibrium Sb (III) concentration (mg/L).

To test the effect of pH on the adsorption of Cs (I), 0.01 g TNS was added to a 100 mL solution with an initial cesium concentration of 10 mg/L, and a negligible 0.1 mol/L HCl or NaOH solution was added to adjust the concentration of each solution. The pH value ranged from 2 to 9. Other conditions such as temperature, rotation speed, and reaction time were the same as the above conditions.

In order to study the effect of TNS dosage on the adsorption of Cs (I), 0.005, 0.010, 0.015, 0.020, 0.025, 0.030, 0.035, and 0.040 g TNS was added to 100 mL of Cs (I) neutralization solution with a concentration of 10 mg/L. Other conditions such as temperature, rotation speed, reaction time and pH were the same as the above conditions.

To investigate the effect of the ionic strength of the solution on the adsorption of Cs (I), 0.01 g TNS was added to the cesium concentration of 5, 10, 15, 20, 25, 30, 35, and 40. Other conditions such as temperature, rotation speed, reaction time and pH were the same as the above conditions.

For the test of equilibration time, the initial pH of a solution with a Cs (I) concentration of 10 mg/L and 0.01 g adsorbent was adjusted to 5.00 $\pm$ 0.05 with 0.1 mol/L HCl or 0.1 mol/L NaOH. Then, the Erlenmeyer flask containing these mixtures was put into an air bath constant temperature shaker to react for 5, 10, 15, 20, 25, 30, 60, 90, and 120 minutes, and then taken out. Other conditions such as temperature, speed, and PH were the same as the above conditions.

3. RESULTS AND DISCUSSION

3.1. Characterization of TNS

Figure 1 is a transmission electron microscope image of TNS under different magnifications. It can be clearly seen from the figure that TNS is a flake structure. Under a high-power transmission electron microscope (Figure 1(a)), it can be seen that there is a layered structure between the TNS. It shows that by changing the synthesis conditions (temperature, time and ratio), the flake titanate nanomaterials were successfully synthesized. The reason is that the granular TiO_2 exfoliates into a flake structure under alkaline hydrothermal conditions. During the reaction, a large number of Ti-O bonds are broken, causing the TiO_2 nanoparticles to be peeled off into smaller planar nanoplates. These smaller planar nanoparticles flakes are combined together to form larger flat nano flakes (Lu *et al.* 2015), and finally Na (I) is embedded in the titanate nano-layers by NaOH alkalization, which provides a site for ion exchange.

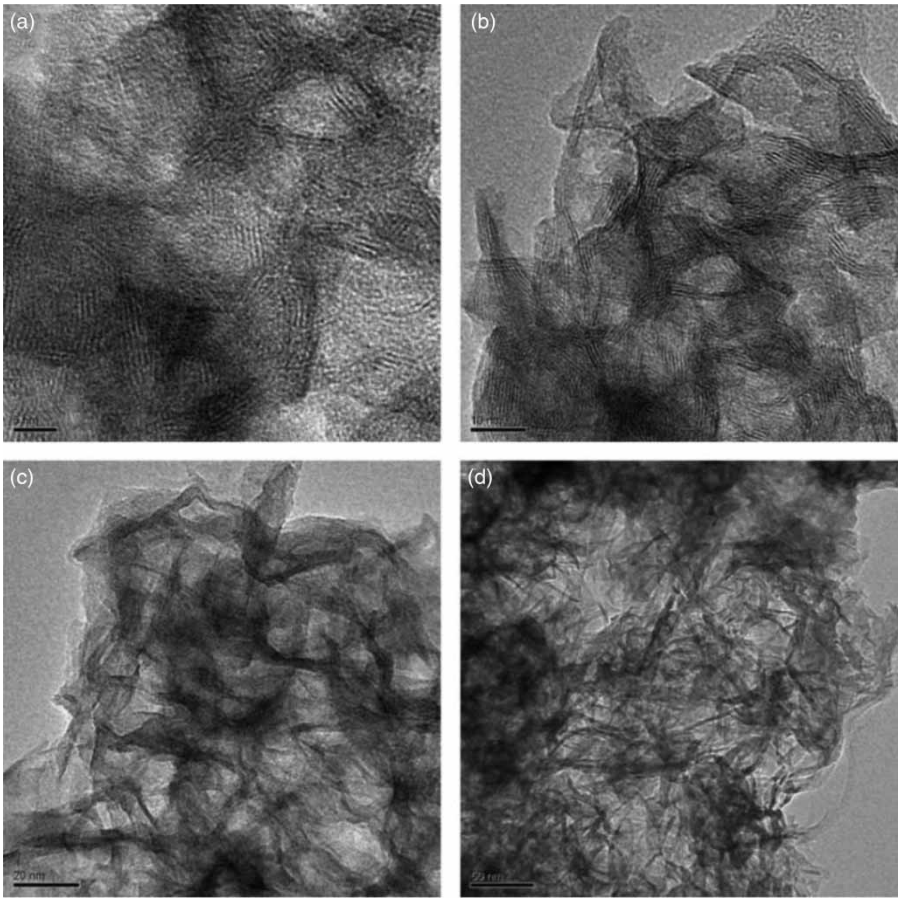

Figure 1 | TNS powders with different magnification, (a) 5 nm; (b) 10 nm; (c) 20 nm; (d) 100 nm.

The N_2 adsorption/desorption isotherm of TNS is shown in Figure 2. The specific surface area of TNS measured by nitrogen adsorption is 325.08 m^2/g, and the main mesopore volume is 1.1 cm^3/g, which is almost consistent with the existing research (Lu *et al.* 2015). According to the graph, the nitrogen adsorption/desorption

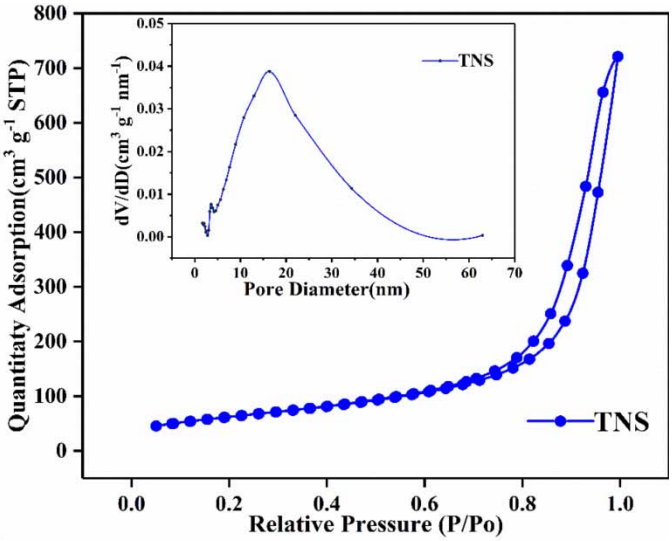

Figure 2 | N_2 sorption/desorption isotherm of TNS.

isotherm of TNS is of type IV, with a larger H3 hysteresis loop, classified by IUPAC, which represents the mesoporous structure. The mesopores are mainly derived from the gaps of aggregated nanosheets (Pekárek & Veselý 1972), indicating that TNS is a mesoporous material. The ion exchange schematic diagram of adsorption process was illustrated in Figure 8.

3.2. Influence of pH value of solution

It can be seen from Figure 3(a) that when pH = 5, the adsorption effect of TNS on Cs (I) is best; the removal rate is 87.91%, and the adsorption capacity can reach 87.91 mg/g. The stronger the acidity or alkalinity of the solution, the worse the removal rate. The Zeta potential diagram of TNS shows (Ting *et al.* 2015) that it is positively charged under acidic conditions and produces a repulsive force with Cs (I) in the solution, so the adsorption effect is poor. In addition, under acidic conditions, the H_3O+ in the solution will compete with Cs (I), resulting in poor adsorption. Na+ is embedded in the layers of TNS adsorbents, and ion exchange occurs with Cs (I) during the adsorption process. Therefore, the main adsorption mechanism of TNS on Cs (I) is ion exchange.

3.3 Effect of adsorbent dosage

Figure 3(b) shows that as the concentration of TNS increases, Cs (I) removal efficiency increases, the increase becoming smaller and smaller. When the concentration is 0.05 g/L of TNS, Cs (I) removal rate was 41.98%, with an adsorption quantity of 83.86 mg/g; when the concentration increased from 0.05 g/L to 0.2 g/L, the Cs removal rate increased by 42.46% and the adsorption capacity decreased by 41.93 mg/g. When the concentration increased from 0.2 g/L to 0.4 g/L, the change of removal efficiency and adsorption capacity decreased significantly, with the increase and decrease of 12.05% and 17.95 mg/g respectively. The main reason is that as the concentration of TNS increases, the adsorption sites are increased, thus increasing the effective collision, so the removal rate also increases. On the contrary, the unit adsorption capacity of TNS decreases with the increase of the concentration, mainly because the content of Cs (I) is constant, the concentration of the adsorbent becomes larger, and there will be redundant active sites in the solution to a certain extent. Studies have also shown that, when the adsorbent concentration increases, collisions and focusing with each other are increased, and there are fewer active sites per unit mass of the adsorbent, so the unit adsorption capacity will also decrease (Sangvanich *et al.* 2010a). After comprehensive consideration, it was finally determined that the concentration of TNS in this experiment was 0.1 g/L.

3.4. Effect of temperature

The effect of temperature on the adsorption performance of TNS is shown in Figure 3(c). As the temperature increases, the removal rate of Cs (I) by TNS increases. When the temperature is 5 °C, the removal rate of Cs (I) is 81.04%. When the temperature rises to 45 °C, the removal rate is 89.9%, and the removal rate increase is 8.86%. The overall analysis increase is not very large. The main reason why the removal rate increases with the increase of temperature is that the activation energy of the adsorbate increases with the increase of temperature,

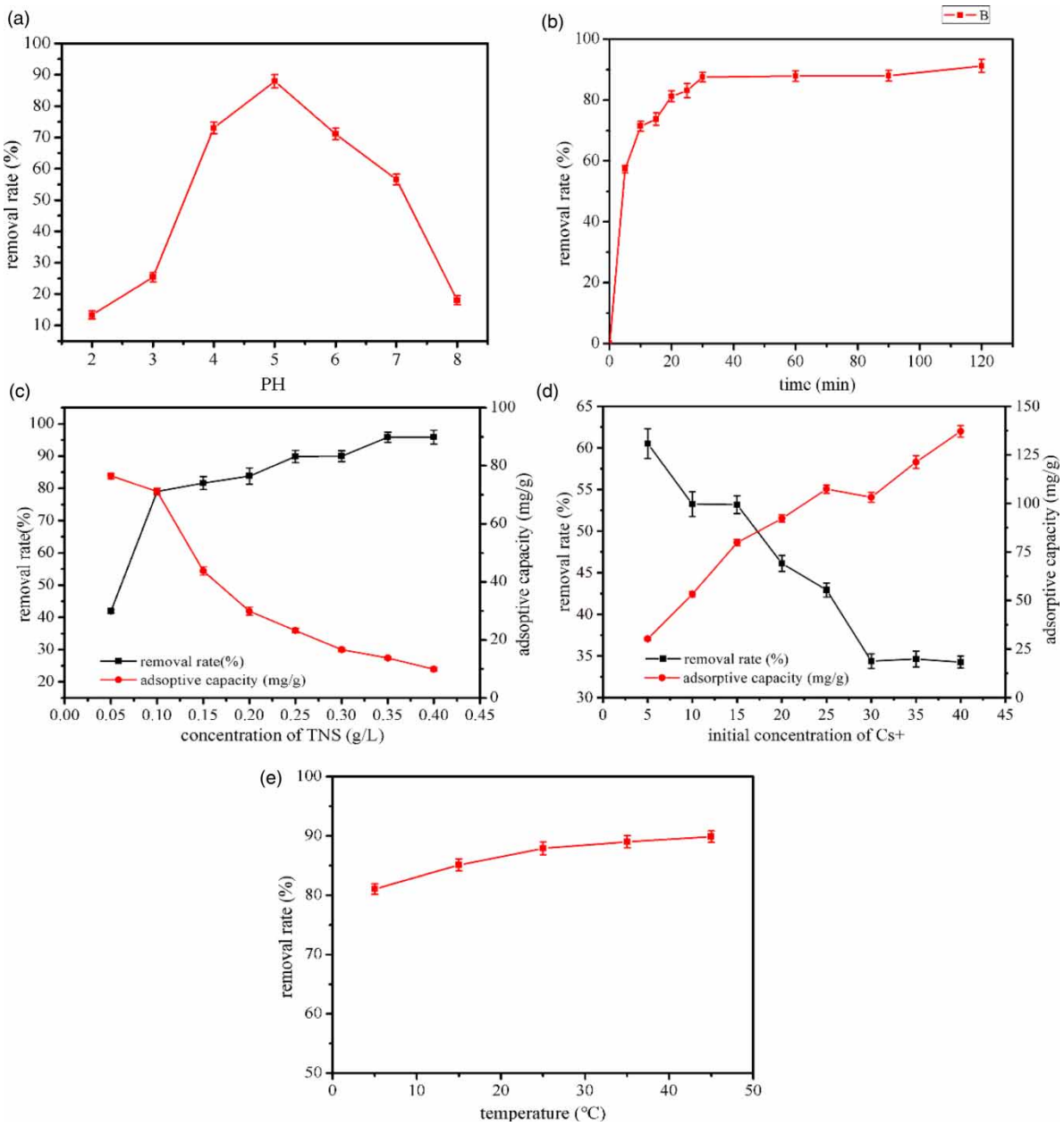

Figure 3 | Effect of (a) solution pH; (b) adsorbent dosage; (c) reaction time; (d) initial concentration; (e) temperature.

which intensifies its movement speed and increases the effective collision of Cs (I) with the adsorbent (Lu *et al.* 2018). Based on practical applications, 25 °C was selected as the experimental temperature of this study.

3.5. Influence of initial concentration of cesium ions in solution

The effect of the initial concentration of Cs (I) on the adsorption performance of TNS is shown in Figure 3(d). The removal rate of Cs (I) by TNS gradually decreases as the initial concentration increases. However, with the increase of the initial concentration of Cs (I), the unit adsorption capacity of TNS increases instead, which is consistent with the description of many adsorption-related studies (Rangwani *et al.* 2018; Sunil *et al.* 2018). It can be seen from the figure that when the initial concentration of Cs (I) is 5 mg/L, the removal rate of Cs (I) by TNS is 60.52%, and its unit adsorption capacity is 30.26 mg/g; when the initial Cs (I) concentration in the reaction system increased to 40 mg/L, the removal rate of Cs (I) by TNS dropped to 34.27%, but the unit adsorption capacity of TNS increased to 137.08 mg/g. This is because as the initial concentration of Cs (I) in the reaction system increases, the effective collision with the adsorbent TNS will increase. In addition, its concentration gradient ($\Delta Q = Qe - Qt$) also increases accordingly, and it produces a stronger effect under the action of external force shaking, which provides energy for Cs (I) to move between TNS layers. These two effective forces increase

the unit adsorption capacity of TNS (Lu *et al.* 2018); the active sites for Cs (I) in the quantitative adsorption material TNS are also certain, when the limited active sites are all occupied by Cs (I) or the concentration is too low, when it fails to collide with the adsorbent effectively, the removal efficiency decreases instead.

3.6. Effect of reaction time

The effect of reaction time on TNS adsorption performance is shown in Figure 3(e). It is roughly divided into three stages, initial stage (0–20 min), very fast TNS adsorption of Cs (I), removal rate of 81.27%; with the increase of CS (I) content on the surface of TNS, the mass transfer power decreases and the adsorption rate also decreases, and the reaction is in the intermediate stage (20–30 min); after an adsorption time of 30 min, the adsorption rate was basically unchanged, and the removal rate was stable at about 88%, which was in the adsorption equilibrium stage. In the initial stage the surface diffusion has a leading role, a large number of Cs (I) with Na + ion exchange complexation with titanium keys; in the intermediate stage, the content of adsorbents and the adsorption sites on the surface of the adsorbents became less, the adsorbents began to diffuse inward, and the reaction rate slowed down. Finally, the reaction reaches adsorption equilibrium and the removal efficiency does not change.

3.7. Ion exchange experiment analysis

In order to explore the amount of Na (I) released during the adsorption process, this experiment measured the Na (I) concentration before and after the adsorption of Cs (I), and was measured three times to get the average value. The test results are shown in Table S1 (Supplementary Information). The contribution rate of Na (I) in the adsorption reaction was 97.6%, indicating that the main mechanism of TNS adsorption of Cs (I) is ion exchange, and there is also surface complexation.

3.8. Adsorption kinetics

Substitute the experimental data of Cs (I) adsorption time and adsorption amount into the pseudo-first order model and pseudo-second order model, and the fitting results are shown in Figure 4(a) and 4(b). The results show that the fitting correlation of the pseudo-first order model is poor, and the correlation coefficient $R^2 = 0.8929$. The equilibrium adsorption capacity is 10.794 mg/g, and the experimental equilibrium adsorption capacity is 96.051 mg/g, which deviates from the experimental value by 88.76%. In comparison, the pseudo-second order model has the best fitting effect, with a correlation coefficient $R^2 = 0.9995$. The results in the table show that the equilibrium adsorption capacity is 91.039 mg/g, which deviates from the experimental value by 5.21%, indicating that the pseudo-second order model is more suitable for the study of the adsorption kinetics of Cs (I) by TNS. The reaction is mainly chemical adsorption.

3.9. Adsorption isotherms and thermodynamics

In this study, the Freundlich model and Langmuir model were used to analyze the adsorption behavior of TNS on Cs. Their models can be exhibited as follows (Debnath *et al.* 2020).

Langmuir model:

$$\frac{C_e}{q_e} = \frac{1}{K_L q_m} + \frac{C_e}{q_m} \tag{3}$$

Freundlich model:

$$lnq_e = lnK_F + \frac{1}{n_F} lnC_e \tag{4}$$

Temkin model:

$$q_e = K_1 lnK_2 + K_1 lnC_e \tag{5}$$

where C_e is the equilibrium concentration of Cs (I) (mg/L), q_e and q_m are the equilibrium adsorption capacity and the maximum adsorption capacity respectively (mg/g), K_L and K_F are the adsorption constants of the Langmuir model and Freundlich model, n_F is the Freundlich model constant, K_1 is related to the heat of adsorption (L/g) and K_2 is the dimensionless Temkin isotherm constant. Figure 4(c)–4(e) fitting result shows that the Langmuir model fitting correlation coefficient is $R^2 = 0.9903$, which is better than Freundlich model ($R^2 = 0.9844$) and Temkin model ($R^2 = 0.9804$). This indicates that the adsorption of Cs (I) by TNS is monomolecular adsorption,

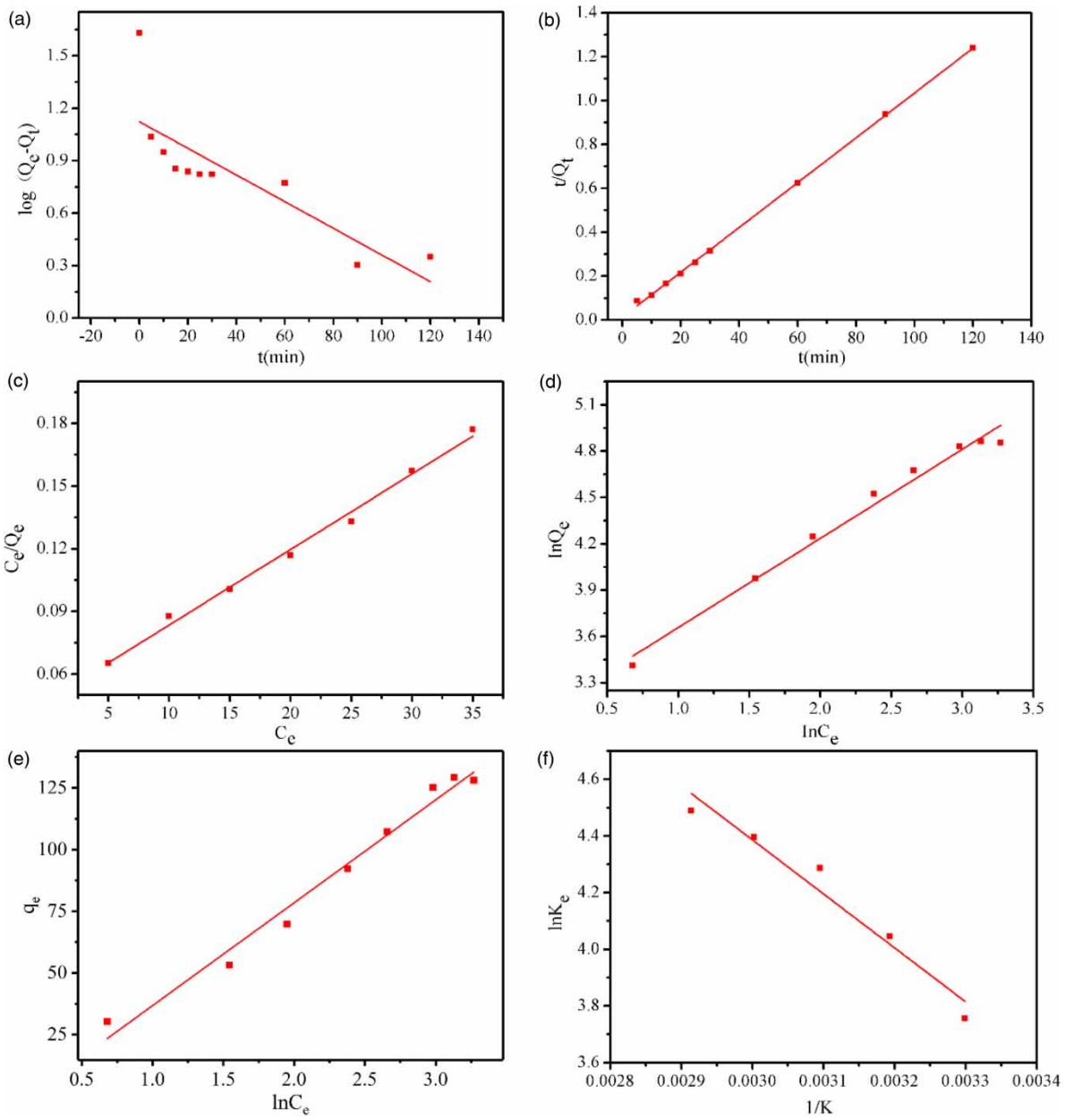

Figure 4 | (a) Pseudo-first-order model, (b) pseudo-second-order model, (c) Langmuir model, (d) Freundlich model and (e) Temkin model and (f) plot of ln K_e vs. 1/T for the adsorption of Cs (I).

and there is no interaction between adsorbate molecules, and the energy is evenly distributed on the surface of the adsorbate. The Freundlich model fitting results show that the TNS and Cs (I) between the strong force, adsorption reaction occurs easily. Langmuir model fitting results show that the maximum adsorption capacity of Cs (I) TNS is 200.00 mg/g, when the initial concentration of Cs (I) for 10 mg/L, K_L is 0.08; within the scope of the 0–1, it is seen that powder TNS affinity of Cs (I) is bigger, which is conducive to the adsorption reaction.

In order to further study Cs (I) adsorption behavior on TNS, basic thermodynamic parameters were calculated in Table S2 according to the experimental data as follows (Li *et al.* 2015; Li *et al.* 2019):

$$lnK_e = \frac{\Delta S}{R} - \frac{\Delta H}{RT} \tag{6}$$

$$K_d = \frac{q_e}{C_e} \tag{7}$$

$$\Delta G = \Delta H - T\Delta S \tag{8}$$

where ΔS, ΔH and ΔG represent the entropy change, enthalpy change and free energy change respectively, K_d is the distribution coefficient. R is the gas constant (8.314×10^{-3} Kj/(mol·K)). The basic thermodynamic parameters, free energy change (ΔG), enthalpy change (ΔH) and entropy change (ΔS) of Cs (I) are listed in Table S2 by calculation based on experimental data. Figure 4(c) and 4(d) show that K_e increases with temperature in the range of 293.15–333.15 K. The calculated ΔG are all less than 0, indicating that the adsorption reaction of Cs (I) can proceed spontaneously and forward, and with the increase of temperature |ΔG| becomes larger, indicating that the temperature rise is beneficial to the reaction. The fitting ΔH > 0 indicates that the process of TNS adsorbing Cs (I) is an endothermic reaction. The value of ΔS obtained by fitting is positive but small, indicating that the disordered movement of Cs (I) in the solution is enhanced, but the degree of enhancement is relatively weak (Wang *et al.* 2019).

3.10. FTIR analysis before and after adsorption

The infrared test results before and after TNS adsorption of Cs (I) are shown in Figure S1 (Supplementary Information). Before adsorption, there are obvious functional group characteristic peaks at 489 cm^{-1}, 920 cm^{-1}, 1,373 cm^{-1}, 1,639 cm^{-1}, and 3,359 cm^{-1}. Among them, the peak at 489 cm^{-1} is the characteristic peak of Ti-O octahedral tensile vibration, the peak at 1,373 cm^{-1} is formed by the hydroxyl (-OH) tensile vibration, and the peak at 1,639 cm^{-1} is the carboxyl (-COOH) shock peak, which indicates the presence of hydroxyl and carboxyl groups on the surface of TNS. The peak at 920 cm^{-1} indicates the presence of Na-O in TNS (Zhao *et al.* 2019) After adsorption, the spectrum shows that the peak intensity at 3,359 cm^{-1} and 1,639 cm^{-1} increases, which is due to the formation of carboxyl (-COOH) or hydroxyl (-OH) stretching vibrations. The Na-O peak at 920 cm^{-1} becomes weaker, while the OH peak at 1,373 cm^{-1} disappears. Correspondingly, a new peak appears at 658 cm^{-1}, indicating Na (I) in TNS and Cs (I) in the reaction system. The ion exchange reaction occurs, and H^+ also participates in the adsorption reaction. The above results indicate that TNS successfully adsorbed Cs (I). The FTIR spectrum after adsorption shows that some characteristic peaks are still very strong, but the peak position has slightly shifted, indicating that the chemical composition, atomic bonding mode and state of TNS have not changed significantly after adsorption.

After comparing the FTIR spectra before and after the reaction, a new absorption peak appeared during the adsorption process but an old absorption peak also disappeared, and some absorption peaks were slightly shifted. According to the analysis results in Table S3, the displacement of each functional group indicates that Cs (I) has a complex reaction with the active adsorption site on TNS to form a surface complex.

3.11. SEM and EDS analysis before and after adsorption

The results of the TNS surface scan before adsorption are shown in Figure 5(a), and the results show that the distribution of Ti, Na, and O elements is relatively uniform. The surface scan results after TNS adsorption of Cs (I) are shown in Figure 5(b). The elements Ti and O undergo almost no change, the distribution is uniform and the content signal does not change significantly from before the reaction, but the content signal of Na element is significantly weaker. At the same time, the signal of Cs (I) clearly appeared in the figure. This shows that during the adsorption reaction, Na element participates in the reaction and ion exchanges with Cs (I). This is consistent with the infrared characterization results, indicating that TNS does indeed combine with Cs (I).

The surface element changes were analyzed by scanning the TNS surface before and after the reaction. As shown in Figure 5(c) and 5(d), the three elements of Ti, O and Na were detected on the TNS surface before the reaction, but cesium was not detected. It can be seen that the peak of the Na element becomes weaker, and the peak of Cs (I) appears, indicating that Na (I) and Cs (I) undergo ion exchange during the adsorption process, which is consistent with the surface scan and infrared results. Among them, the content of Cs (I) was 15.75%.

3.12. XRD analysis before and after adsorption

The XRD pattern of TNS is shown in Figure 6. Before adsorption, three distinct characteristic peaks appear at $2\theta = 9.6°$, 26.8° and 47.6°, which belong to the crystal titanate diffraction. TNS is composed of triad [TiO_6] octahedrons, interlaminar Na (I) and H (I), and interlaminar Na (I) or H (I) are its main adsorption sites. $2\theta = 9.6°$ is the interlaminar diffraction peak of titanate, indicating the existence of an intermediate interlayer (Liu *et al.* 2013). After adsorption, the peak intensity at $2\theta = 9.6°$ decreased significantly, indicating that the adsorption intensity of TNS decreased, and the interlayer Na (I) and Cs (I) exchanged ions. In addition, $2\theta = 26.8$ ° of the characteristic peak of sodium titanate was weak, which says that the content of Na (I) reduced (Lee *et al.* 2008), showing that the TNS Cs (I) is the main adsorption mechanism of ion exchange.

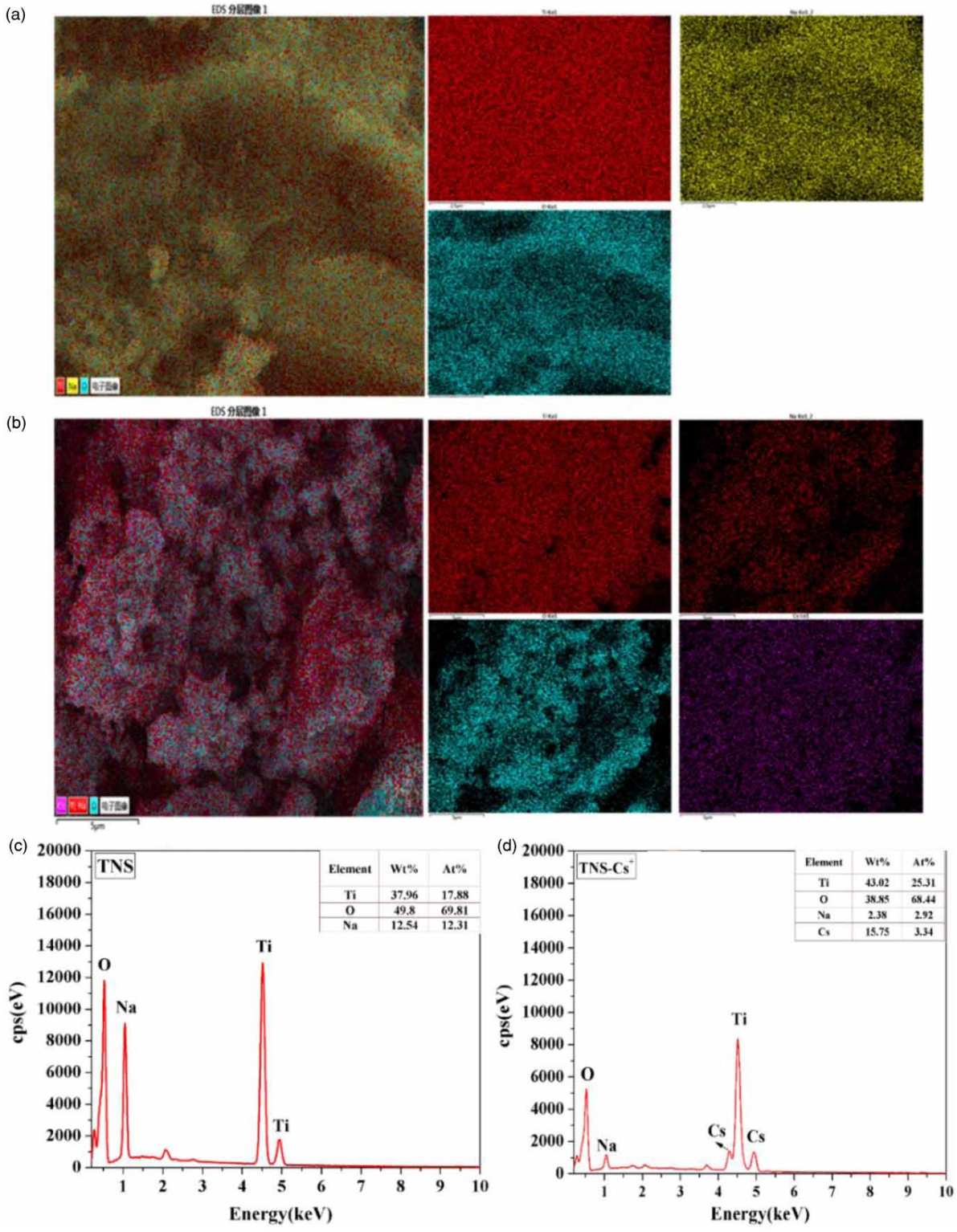

Figure 5 | SEM and EDS image of TNS (a) before adsorption and (b) after adsorption, EDS total spectra of TNS (c) before adsorption and (d) after adsorption.

3.13. XPS analysis before and after adsorption

According to XPS spectra (Figure 7(a)), before adsorption, characteristic peaks of Na, O and Ti appeared in the range of 400–1,100 eV, and these three elements were the main elements of TNS. As shown in Figure 7(b), the peaks located at 457.98 eV and 463.68 eV are Ti-O and Ti-Ti bonds respectively. Through the strength of

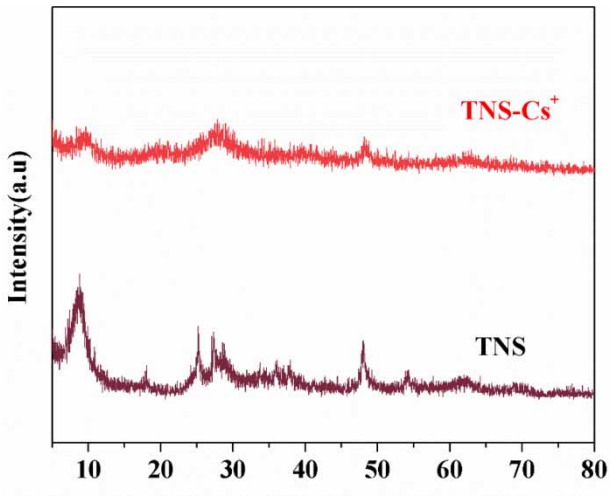

Figure 6 | XRD spectra of TNS before and after Cs (I) adsorption.

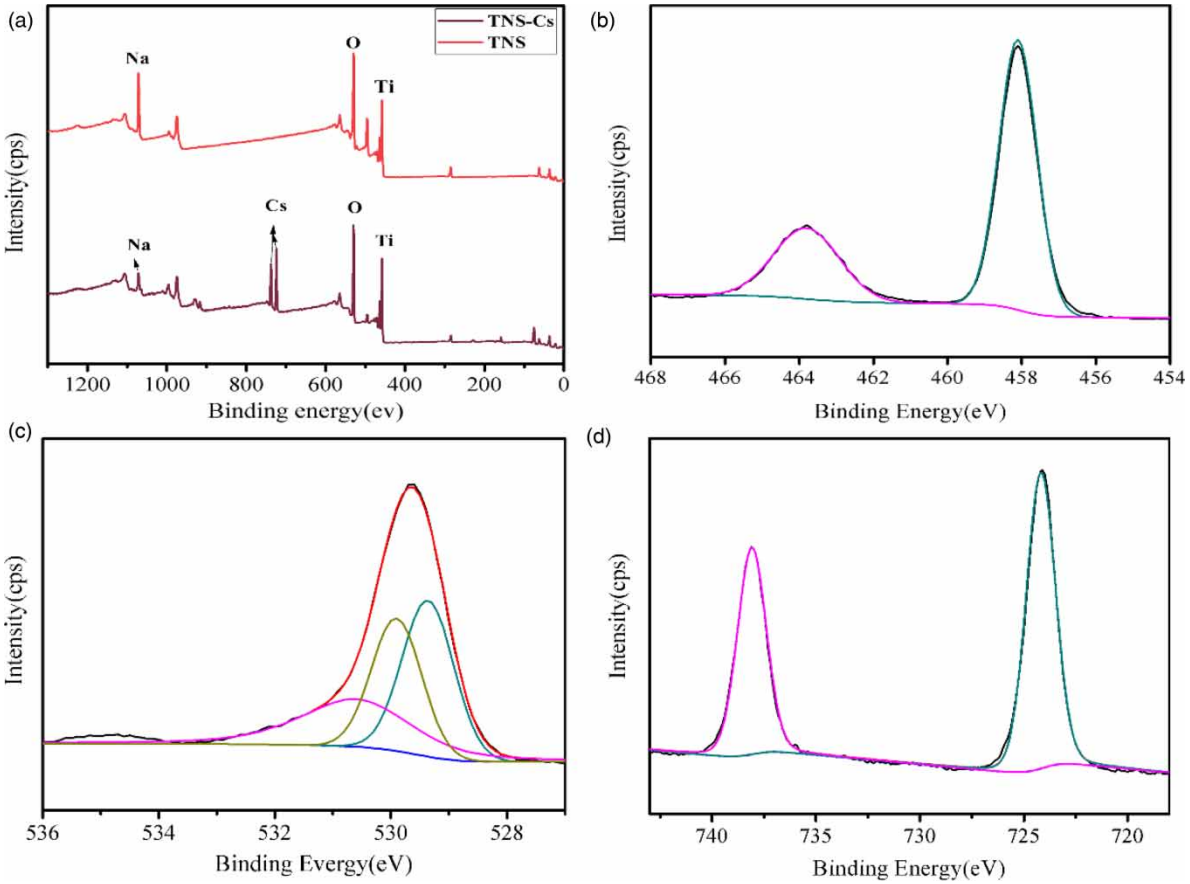

Figure 7 | XPS spectra of TNS, (a) overall spectra (b) Ti 2p peaks (c) O 1s peaks (d) Cs 3 d peaks.

the peak, it can be inferred that there are more Ti-O bonds, and the difference between the two bonds is 5.7 eV. The O 1s spectrum is shown in Figure 7(c). The main peak of 529.9 eV was assigned to Ti-OH, and the peaks of 529.36 eV and 530.6 eV corresponded to Ti-O and $Na_2Ti_3O_7$ respectively (Liu *et al.* 2021). After adsorption, O and Ti, two kinds of element characteristic peak positions and intensities did not significantly change, but the element characteristic peak of Na significantly weakened, and in the 722.68 eV and 736.68 eV bimodal characteristics (shown in Figure 7(d)). The above suggests that Na (I) in the TNS and solution of Cs (I) has an ion exchange function, and the structure of the TNS before and after reaction shows almost no change.

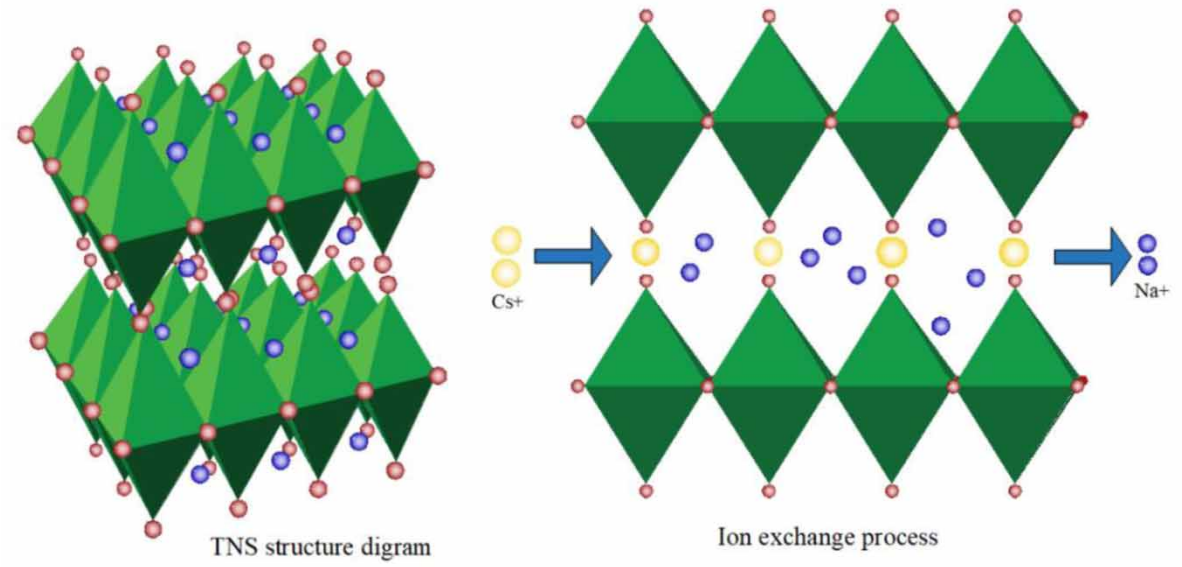

Figure 8 | TNS and CS (I) ion exchange schematic.

3.14. Regeneration and reusability of TNS

Recycling performance is an important factor in evaluating TNS adsorption performance in practical application. In the adsorption-desorption experiment, 0.5 M NaOH was used as the eluent to desorb Cs (I) from TNS. Five cycles of adsorption-desorption were repeated with the same sample of adsorbent. As can be seen from Figure S3, after five adsorption-desorption cycles, the removal rate of Cs (I) dropped from the initial 87.95% to 81.54%, and the adsorption performance did not significantly decline. The results show that TNS can be used as an efficient adsorbent for Cs (I).

4. CONCLUSION

The layered titanate nanometer sheet (TNS) adsorbents were prepared by controlling the process conditions of hydrothermal synthesis. TNS to Cs (I) has a larger adsorption capacity, at the pH = 5.00 ± 0.05, $C_0 = 10$ ppm and $C_{TNS} = 0.1$ g/L the removal rate reached 88%. The TNS on Cs (I) adsorption process can be divided into fast adsorption (0–10 min), slow adsorption (10–20 min) and equilibrium adsorption; three stages. After the rapid adsorption stage, the removal rate can reach over 85%, and the adsorption equilibrium can be reached at around 20 min, which is most consistent with the quasi-second-order kinetic model, $R^2 = 0.9998$, indicating that the reaction is a heterogeneous diffusion process. A TNS Cs (I) process in line with the Langmuir adsorption model is proposed, showing the TNS to Cs (I) adsorption is monolayer adsorption, with no interaction between adsorbate molecule, energy is uniformly distributed on the surface adsorption material. Langmuir model fitting to get the maximum adsorption capacity of Cs (I) of 200.00 mg/g. FTIR and SEM-EDX characterization results showed that Na element was involved in the adsorption process. TNS XRD and XPS spectra showed that interlayer Na (I) and Cs (I) ion exchange action results in the decrease of the content of Na (I), so the TNS to Cs (I) is the main adsorption.

ACKNOWLEDGEMENT

The authors are very grateful to the National Key Research and Development Program of China (No. 2016YFC1402504) for the funding support for this research.

DATA AVAILABILITY STATEMENT

All relevant data are included in the paper or its Supplementary Information.

REFERENCES

Abusafa, A. & Yücel, H. 2002 Removal of 137 Cs from aqueous solutions using different cationic forms of a natural zeolite: clinoptilolite. *Separation and Purification Technology* **28**(2), 103–116.

Amadelli, R., Maldott, A., Sostero, S. & Carassiti, V. 1992 Cheminform abstract: photodeposition of uranium oxides onto TiO_2 from aqueous uranyl solutions. *ChemInform* **23**(1), 342–343.

Bhowmik, M., Debnath, A. & Saha, B. 2019 Fabrication of mixed phase $CaFe_2O_4$ and $MnFe_2O_4$ magnetic nanocomposite for enhanced and rapid adsorption of Methyl orange dye: statistical modeling by neural network and response surface methodology. *Journal of Dispersion Science and Technology* **41**(13), 1937–1948.

Chen, P.-Y. 2007 The assessment of removing strontium and cesium cations from aqueous solutions based on the combined methods of ionic liquid extraction and electrodeposition. *Electrochimica Acta* **52**(17), 5484–5492.

Chen, X. & Li, Y. 2019 Research progress on separation of rubidium and cesium by ion exchange. *Inorganic Chemicals Industry* **51**(4), 6–9.

Chen, R., Tanaka, H., Kawamoto, T., Asai, M., Fukushima, C., Na, H., Kurihara, M., Watanabe, M., Arisaka, M. & Nankawa, T. 2013 Selective removal of cesium ions from wastewater using copper hexacyanoferrate nanofilms in an electrochemical system. *Electrochimica Acta* **87**, 117–125.

Deb, A., Debnath, A. & Saha, B. 2020 Ultrasound-aided rapid and enhanced adsorption of anionic dyes from binary dye matrix onto novel hematite/polyaniline nanocomposite: response surface methodology optimization. *Applied Organometallic Chemistry* **34**(2), 1357581.

Debnath, A., Bera, A., Chattopadhyay, K. K. & Saha, B. 2017 Facile additive-free synthesis of hematite nanoparticles for enhanced adsorption of hexavalent chromium from aqueous media: kinetic, isotherm, and thermodynamic study. *Inorganic and Nano-Metal Chemistry* **47**(12), 1357581.

Debnath, B., Majumdar, M., Bhowmik, M., Bhowmik, K. L., Debnath, A. & Roy, D. N. 2020 The effective adsorption of tetracycline onto zirconia nanoparticles synthesized by novel microbial Green technology. *Journal of Environmental Management* **261**, 110235.

Grandjean, A., Delchet, C., Causse, J., Barré, Y., Guari, Y. & Larionova, J. 2016 Effect of the chemical nature of different transition metal ferrocyanides to entrap Cs. *Journal of Radioanalytical and Nuclear Chemistry* **307**(1), 427–436.

Iwanade, A., Kasai, N., Hoshina, H., Ueki, Y., Saiki, S. & Seko, N. 2012 Hybrid grafted ion exchanger for decontamination of radioactive cesium in Fukushima Prefecture and other contaminated areas. *Journal of Radioanalytical and Nuclear Chemistry* **293**(2), 703–709.

Jiang, C., Wang, S., Song, C., Sun, Y., Wang, Q. & Xu, S. 1995 Removal of Cs from high level rdioative liquid waste with potassium titanium hexacyanoferrate. *Journal of Nuclear and Radiochemistry* **2**, 99–104.

Kadam, A. A., Jiseon, J. & Sung, L. D. 2016 Facile synthesis of pectin-stabilized magnetic graphene oxide Prussian blue nanocomposites for selective cesium removal from aqueous solution. *Bioresource Technology* **216**, 391–398.

Lee, C.-K., Lin, K.-S., Wu, C.-F., Lyu, M.-D. & Lo, C.-C. 2008 Effects of synthesis temperature on the microstructures and basic dyes adsorption of titanate nanotubes. *Journal of Hazardous Materials* **150**(3), 494–503.

Li, J., Yang, X., Bai, C., Tian, Y., Li, B., Zhang, S., Yang, X., Ding, S., Xia, C., Tan, X., Ma, L. & Li, S. 2015 A novel benzimidazole-functionalized 2-D COF material: synthesis and application as a selective solid-phase extractant for separation of uranium. *Journal of Colloid and Interface Science* **437**, 211–218.

Li, T., He, F., Jiang, D., Wang, G., Wang, G. & Dai, Y. 2016 Cesium adsorption on a multi-metal Prussian Blue analogue Copper-Nickel-Cobalt Hexacyanoferrate. *Materials Review* **30**(11), 71–76.

Li, X., Wang, Z., Liang, H., Ning, J., Li, G. & Zhou, Z. 2019 Chitosan modification persimmon tannin bioadsorbent for highly efficient removal of Pb(II) from aqueous environment: the adsorption equilibrium, kinetics and thermodynamics. *Environmental Technology* **40**(1), 112–124.

Liu, W., Wang, T., Borthwick, A. G. L., Wang, Y., Yin, X., Li, X. & Ni, J. 2013 Adsorption of Pb^{2+}, Cd^{2+}, Cu^{2+} and Cr^{3+} onto titanate nanotubes: competition and effect of inorganic ions. *Science of the Total Environment* **456–457**, 171–180.

Liu, C., Li, Y., Wang, X., Li, B., Zhou, Y., Liu, D., Liu, D. & Liu, S. 2021 Efficient extraction of antimony(III) by titanate nanosheets: study on adsorption behavior and mechanism. *J Ecotoxicology and Environmental Safety* **207**, 111271.

Lu, D., Fang, P., Liu, X., Zhai, S., Li, C., Zhao, X., Ding, J. & Xiong, R. 2015 A facile one-pot synthesis of TiO_2-based nanosheets loaded with MnxOy nanoparticles with enhanced visible light–driven photocatalytic performance for removal of Cr(VI) or RhB. *Applied Catalysis B: Environmental* **179**, 558–573.

Lu, T., Zhu, Y., Wang, W., Qi, Y. & Wang, A. 2018 Interconnected superporous adsorbent prepared via yeast-based Pickering HIPEs for high-efficiency adsorption of Rb +, Cs + and Sr^{2+}. *Chemical Engineering Journal*.

Pekárek, V. & Veselý, V. 1972 Synthetic inorganic ion exchangers-II salts of heteropolyacids, insoluble ferrocyanides, synthetic aluminosilicates and miscellaneous exchangers. *Talanta* **19**(11), 1245–1283.

Rangwani, S., Howarth, A. J., DeStefano, M. R., Malliakas, C. D., Platero-Prats, A. E., Chapman, K. W. & Farha, O. K. 2018 Adsorptive removal of Sb(V) from water using a mesoporous Zr-based metal–organic framework. *Polyhedron* **151**, 338–343.

Sangvanich, T., Sukwarotwat, V., Wiacek, R. J., Grudzien, R. M., Fryxell, G. E., Addleman, R. S., Timchalk, C. & Yantasee, W. 2010a Selective capture of cesium and thallium from natural waters and simulated wastes with copper ferrocyanide functionalized mesoporous silica. *Journal of Hazardous Materials* **182**(1–3), 225–231.

Sangvanich, T., Sukwarotwat, V., Wiacek, R. J., Grudzien, R. M., Fryxell, G. E., Addleman, R. S., Timchalk, C. & Yantasee, W. 2010b Selective capture of cesium and thallium from natural waters and simulated wastes with copper ferrocyanide functionalized mesoporous silica. *Journal of Hazardous Materials* **182**(1), 225–231.

Sunil, K., Karunakaran, G., Yadav, S., Padaki, M., Zadorozhnyy, V. & Pai, R. K. 2018 Al-Ti_2O_6 a mixed metal oxide based composite membrane: a unique membrane for removal of heavy metals. *Chemical Engineering Journal* **348**, 678–684.

Thammawong, C., Opaprakasit, P., Tangboriboonrat, P. & Sreearunothai, P. 2013 Prussian blue-coated magnetic nanoparticles for removal of cesium from contaminated environment. *Journal of Nanoparticle Research* **15**(6), 1689.

Thanabalasingam, P. & Pickering, W. F. 1990 Specific sorption of antimony (III) by the hydrous oxides of Mn, Fe, and Al. *Water, Air, and Soil Pollution* **49**(1–2), 175–185.

Ting, W., Wen, L., Xuezhao, L. & Xiaolin, J. 2015 Simultaneous removal of Cr(VI) and Cr(III) by titanate nanosheets through photocatalysis combined with adsorption. *Environmental Chemistry* **34**(10), 1777–1784.

Vassileva, E., Proinova, I. & Hadjiivanov, K. 1996 Solid-phase extraction of heavy metal ions on a high surface area titanium dioxide (anatase). *Analyst* **122**(5), 607–612.

Wang, X. L., Li, Y., Huang, J., Zhou, Y. Z., Li, B. L. & Liu, D. B. 2019 Efficiency and mechanism of adsorption of low concentration uranium in water by extracellular polymeric substances. *Journal of Environmental Radioactivity* **197**, 81–89.

Yang, J., Jin, Z., Wang, X., Li, W., Zhang, J., Zhang, S., Guo, X. & Zhang, Z. 2003 Study on composition, structure and formation process of nanotube Na_2Ti_2O_4(OH)_2. *Dalton Transactions* 3898–3901.

Yi, R., Ye, G., Wu, F., Wen, M., Feng, X. & Chen, J. 2014 Cheminform abstract: highly efficient removal of ^{137} Cs in seawater by potassium titanium ferrocyanide functionalized magnetic microspheres with multilayer core – shell structure. *RSC Advances* **4**(71), C4RA05397D.

Zakrzewska-Trznadel, G., Harasimowicz, M. & Chmielewski, A. G. 2001 Membrane processes in nuclear technology-application for liquid radioactive waste treatment. *Separation and Purification Technology* **22–23**(1–3), 617–625.

Zhang, D. & Tan, Z. 2013 Synthesis of ammonium molybdophosphate and the uptake behavior for cesium. *Nuclear Technique* **36**(02), 44–47.

Zhao, T., Tang, Z., Zhao, X., Zhang, H., Wang, J., Wu, F., Giesy, J. P. & Shi, J. 2019 Efficient removal of both antimonite (Sb(III)) and antimonate (Sb(V)) from environmental water using titanate nanotubes and nanoparticles. *Environmental Science-Nano* **6**(3), 834–850.

First received 4 February 2021; accepted in revised form 11 June 2021. Available online 25 June 2021